LANGMUIR

Article

pubs.acs.org/Langmuir

Catalytic Reduction of 4-Nitrophenol Using Silver Nanoparticles with Adjustable Activity

Claudia Kästner and Andreas F. Thünemann*

Federal Institute for Materials Research and Testing (BAM), Unter den Eichen 87, 12205 Berlin, Germany

Supporting Information

ABSTRACT: We report on the development of ultrasmall core−shell silver nanoparticles synthesized by an upscaled modification of the polyol process. It is foreseen to use these thoroughly characterized particles as reference material to compare the catalytic and biological properties of functionalized silver nanoparticles. Small-angle X-ray scattering (SAXS) analysis reveals a narrow size distribution of the silver cores with a mean radius of R_c = 3.0 nm and a distribution width of 0.6 nm. Dynamic light scattering (DLS) provides a hydrodynamic radius of R_H = 10.0 nm and a PDI of 0.09. The particles' surface is covered with poly(acrylic acid) (PAA) forming a shell with a thickness of 7.0 nm, which provides colloidal stability lasting for more than 6 months at ambient conditions. The PAA can be easily exchanged by biomolecules to modify the surface functionality. Replacements of PAA with glutathione (GSH) and bovine serum albumin (BSA) have been performed as examples. We demonstrate that the silver particles effectively catalyze the reduction of 4-nitrophenol to 4-aminophenol with sodium borohydride. With PAA as stabilizer, the catalytic activity of 436 ± 24 L g^{-1} s^{-1} is the highest reported in the literature for silver nanoparticles. GSH and BSA passivate the surface substantially, resulting in a catalytic activity of 77.6 ± 0.9 and 3.47 ± 0.50 L g^{-1} s^{-1}, respectively.

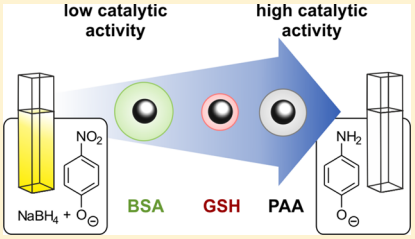

INTRODUCTION

Research on nanosized silver is an increasingly important area in nanoscience with applications ranging from catalysis[1] to medicine.[2] Furthermore, silver is widespread in consumer products in form of silver nanoparticles due to its antibacterial properties.[3] Therefore, the toxicological properties of silver nanoparticles are central in a tremendous amount of studies.

Unfortunately, the results of these studies are extremely diverse. Some investigations conclude that there is no specific nano effect,[4] while others report on the presence of pronounced nano specific effects.[5] This diversity means that no consistent evaluation of the toxicity of silver in form of nanoparticles could be drawn until now. A key problem hindering comparison between these studies may be that they use a wide range of silver nanoparticles. In most of the studies the particles are synthesized in-house or purchased from very different sources, and the physicochemical characterization of the particles is often limited. It has therefore been recognized that nanoscale reference materials for the environmental, health, and safety studies of silver would be helpful for better comparability.[6]

In strong contrast to gold nanoparticles, reports on long-term stable silver nanoparticles are rare because the synthesis of silver nanoparticles with reproducible properties is more difficult than expected.[3] An impressive exception is a type of silver nanoparticles consisting of 44 silver atoms protected by a ligand shell of *p*-mercaptobenzoic acid reported by Desireddy et al.[7] However, this type of particle is too exotic for use as reference materials. Only in a few cases the synthesis requires purely benign chemicals and produces stable particles of uniform size. In this regard the polyol-based procedure is outstanding, which has been improved by Hu et al. by replacing poly(vinylpyrrolidone) with poly(acrylic acid) (PAA).[8]

In this paper long-term stable, ultrasmall silver nanoparticles are synthesized in quantities large enough to make their use in subsequent studies feasible. In addition, the particles are thoroughly characterized in their pristine state and after substitution of PAA as stabilizer with glutathione (GSH) and bovine serum albumin (BSA). Finally, their catalytic properties in the reduction of 4-nitrophenol are demonstrated as a possible application.

RESULTS AND DISCUSSION

Particle Synthesis. We first developed an upscaled variant of the synthesis for the production of PAA-stabilized silver nanoparticles. Details are given in the Materials and Methods section. In contrast to use only 0.1 g of silver nitrate as reported in the original protocol,[8] we attained reproducible results when using up to 2.0 g of silver nitrate in a single batch synthesis with volumes of 350 mL instead of 15 mL. In a second step, we performed a polymer ligand exchange[9] by replacing the PAA on the silver core surfaces of the parent particles ($\mathbf{p}_{PAA}$) with GSH and BSA, resulting in $\mathbf{p}_{GSH}$ and $\mathbf{p}_{BSA}$ particles. The $\mathbf{p}_{PAA}$ are stable for at least 6 months when stored at ambient conditions in the dark at pH values ≥10. In contrast, when using Hu's method for purification of the particles, we found that these $\mathbf{p}_{Hu}$

Received: April 16, 2016
Revised: June 2, 2016
Published: July 5, 2016

DOI: 10.1021/acs.langmuir.6b01477
Langmuir 2016, 32, 7383−7391

particles coat the vessel walls (see Figure SI1 for comparison). An amount of about 50% of $\mathbf{p}_{Hu}$ was found as a gray deposit after 6 months. No deposit was found for $\mathbf{p}_{PAA}$. Therefore, we classify the $\mathbf{p}_{Hu}$ and $\mathbf{p}_{PAA}$ as short-term and long-term stable, respectively. The cause for the difference in stability of $\mathbf{p}_{Hu}$ and $\mathbf{p}_{PAA}$ is likely due to differences in their purification process. Purification of $\mathbf{p}_{Hu}$ includes a centrifugation step while no centrifugation was used for $\mathbf{p}_{PAA}$. Tentatively, we conclude that $\mathbf{p}_{PAA}$ has more stabilizer than $\mathbf{p}_{Hu}$. Thermogravimetric analysis (TGA) measurements were performed to test this hypothesis. The TGA curve of $\mathbf{p}_{PAA}$ shows its mass as a function of temperature (Figure 1, black solid line). The weight reduction

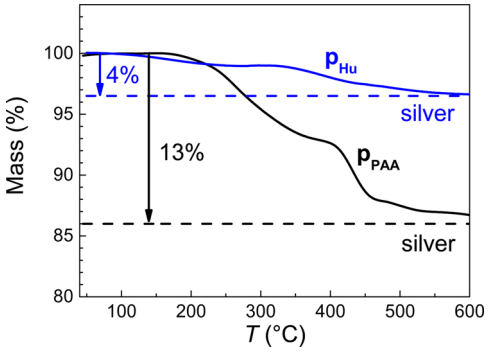

Figure 1. TGA curves of $\mathbf{p}_{PAA}$ showing its mass as a function of temperature (black solid line). The PAA decomposition characterized by two steps is in agreement with results reported in the literature.[10] The $\mathbf{p}_{Hu}$ (blue line) and $\mathbf{p}_{PAA}$ (black line) differ in the loss of PAA ligand, which is 4% and 13%, respectively. Remaining silver is indicated by dashed lines.

occurs in two steps, positioned at 260 and 430 °C for a total of 13 wt %. The remaining amount of 87% silver is indicated as a black dashed line. The two steps of the PAA decomposition are in agreement with the literature.[10] Therein, Lu et al.[10] found two broad degradation steps at around 220−280 °C and at about 430 °C for a PAA with a molar mass of 5000 g mol^{-1}. The TGA curve of $\mathbf{p}_{Hu}$ particles displays a similar trace (blue solid line) but with a much lower total weight reduction of 3−4% (horizontal blue dashed line). It seems to be plausible to interpret that the higher amount of stabilizer found for $\mathbf{p}_{PAA}$ in comparison to $\mathbf{p}_{Hu}$ is the reason for their difference in stability.

The stability of silver nanoparticle dispersions is also affected by pH. When lowering the pH to 7, both the $\mathbf{p}_{PAA}$ and $\mathbf{p}_{Hu}$ particles sediment within an hour. This is expected since the carboxylic acid groups of PAA provide colloidal stability of silver nanoparticle dispersions when they are negatively charged at pH 10. The carboxylic acid groups of PAA can form intermolecular hydrogen bonds and become protonated at pH 7 which is a state in which they cannot provide electrostatic colloidal stabilization. In contrast to $\mathbf{p}_{PAA}$, the $\mathbf{p}_{GSH}$ and $\mathbf{p}_{BSA}$ particles are stable at pH 7, which coincidentally is a clear indication for a successful ligand exchange.

TEM investigations show that $\mathbf{p}_{Hu}$ comprises a core−shell structure[8] whereby spherical silver cores are surrounded by a shell of water-swollen PAA. We assume that $\mathbf{p}_{PAA}$ conforms to this structure with uniform core sizes and different shell thicknesses. Sketches of the structure are shown in Figure 2. We employed multiangle DLS and SAXS as complementary methods for revealing the core−shell structure in detail.

Hydrodynamic Sizes. Multiangle DLS was used to characterize the hydrodynamic radius of the particles as well as aggregation and particle−particle interactions. The reciprocal values of the hydrodynamic radii as a function of the square of the scattering vector are shown in Figure 3a. It can be seen that the $1/R_H$ data of $\mathbf{p}_{Hu}$, $\mathbf{p}_{PAA}$, and $\mathbf{p}_{GSH}$ are independent of q^2, indicating that no aggregation occurs. The data of $\mathbf{p}_{BSA}$ display a slight linear increase with q^2 showing that the size distribution is slightly broader. This indicates that all particles undergo solely translational diffusion, and neither aggregates nor significant particle−particle interactions are present. In contrast, poly-

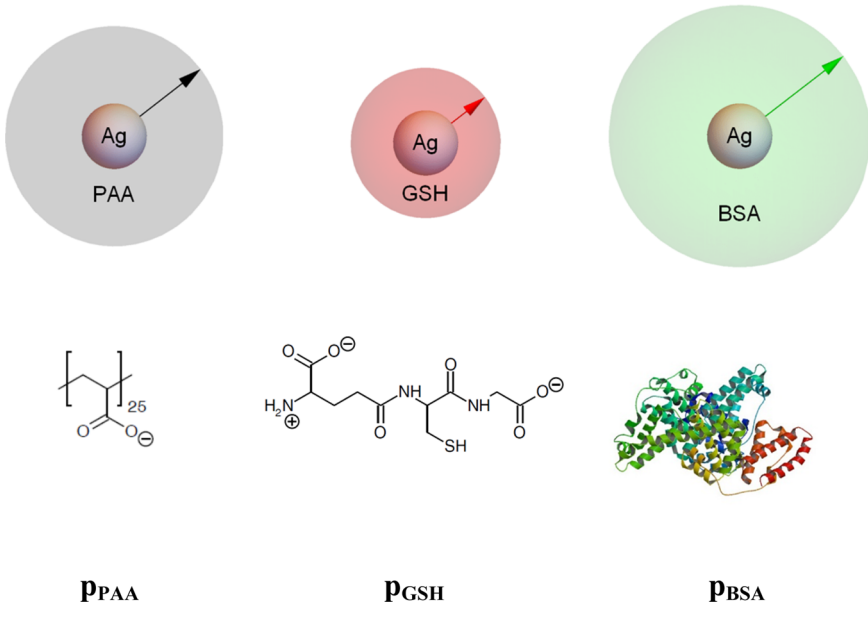

Figure 2. Chemical structures of the (macro)molecules that form a shell around the silver cores and provide long-term stability in dispersion. Shell thicknesses are indicated by arrows. Parent particles $\mathbf{p}_{PAA}$ are stabilized with poly(acrylic acid) (PAA), M_W = 1800 g mol^{-1} (left). The $\mathbf{p}_{GSH}$ are stabilized with glutathione, which is a tripeptide formed by glutamic acid, cysteine, and glycine, M_W = 307 g mol^{-1} (middle). The $\mathbf{p}_{BSA}$ are stabilized with bovine serum albumin (BSA); M_W = 66463 g mol^{-1} (right).

DOI: 10.1021/acs.langmuir.6b01477
Langmuir 2016, 32, 7383−7391

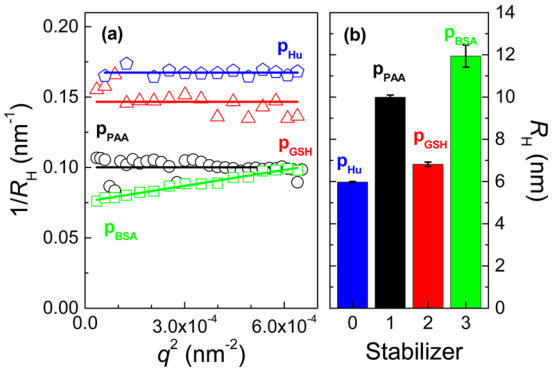

Figure 3. DLS results for silver nanoparticles $\mathbf{p}_{Hu}$, $\mathbf{p}_{PAA}$, $\mathbf{p}_{GSH}$, and $\mathbf{p}_{BSA}$. (a) The reciprocal values of the hydrodynamic radii as a function of q^2 (symbols) were fitted by a linear relationship to determine the extrapolated hydrodynamic radius at zero angle. (b) The fits shown in panel (a) result in R_H = 5.9 ± 0.1 nm ($\mathbf{p}_{Hu}$), 10.0 ± 0.1 nm ($\mathbf{p}_{PAA}$), 6.8 ± 0.1 nm ($\mathbf{p}_{GSH}$), and 11.9 ± 0.5 nm ($\mathbf{p}_{BSA}$).

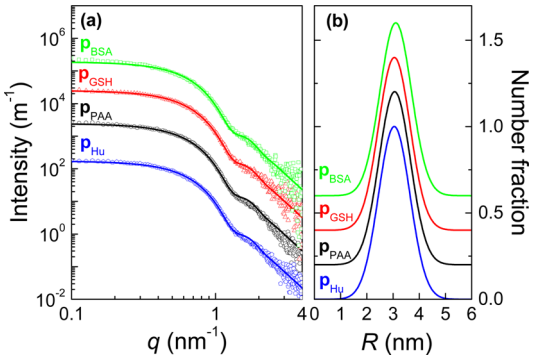

Figure 4. (a) SAXS data and fits of $\mathbf{p}_{Hu}$, $\mathbf{p}_{PAA}$, $\mathbf{p}_{GSH}$, and $\mathbf{p}_{BSA}$ using SASfit[12] resulting in size distributions shown in (b). Mean particle radius is R_n = 3.0 ± 0.1 nm, and the width is σ = 0.6 ± 0.1 nm for $\mathbf{p}_{Hu}$, $\mathbf{p}_{PAA}$, $\mathbf{p}_{GSH}$, and $\mathbf{p}_{BSA}$. The curves in (a) and (b) are shifted vertically for better visibility.

disperse particles or interacting particles display strongly angle-dependent apparent R_h values.[11] Linear fits result in hydrodynamic radii of R_H = 5.9 ± 0.1 nm ($\mathbf{p}_{Hu}$), 10.0 ± 0.1 nm ($\mathbf{p}_{PAA}$), 6.8 ± 0.1 nm ($\mathbf{p}_{GSH}$), and 11.9 ± 0.5 nm ($\mathbf{p}_{BSA}$) from the extrapolated values of $1/R_H$ at q^2 = 0. Without this interpolation we found a continuous increase of the apparent R_h values of p_{BSA} from 10 to 13 nm for 6.4×10^{-4} nm^{-2} > q^2 > 3.5×10^{-4} nm^{-2}. This angular-dependent effect can be much larger as reported, for example, for poly(organosiloxane) nanoparticles, where the apparent R_h change from 22 to 42 nm.[11]

Mean values of the polydispersity index over all angles are PDI = 0.04 ± 0.01 ($\mathbf{p}_{Hu}$), 0.09 ± 0.01 ($\mathbf{p}_{PAA}$), 0.13 ± 0.02 ($\mathbf{p}_{GSH}$), and 0.13 ± 0.02 ($\mathbf{p}_{BSA}$). Note that for angles larger than 150°, the PDI values of all particles were in the range of 0.01−0.04, which could lead to the conclusion that the particles' size distribution is extremely narrow. However, these values can be considered unrealistic, and we therefore averaged PDI values from angles between 40° and 170°.

Core Size Distribution. SAXS was used to determine the size distribution of the particles' silver cores. Since the silver cores scatter 4×10^3 times stronger than the PAA shell, SAXS is an appropriate method for the determination of the core dimensions. The measured SAXS data were fitted assuming a spherical scatterer with a Gaussian size distribution using SASfit[12] (Figure 4a). The resulting number-weighted core size distributions for $\mathbf{p}_{Hu}$, $\mathbf{p}_{PAA}$, $\mathbf{p}_{GSH}$, and $\mathbf{p}_{BSA}$ are near-identical (Figure 4b). The mean number-weighted particle radii are R_n = 3.0 ± 0.1 nm, and the widths of the size distributions are σ = 0.6 ± 0.1 nm, i.e., a relative width of σ_r = 20 ± 3%. When using Glatter's data evaluation method for determination of particle size distributions, which is based on the indirect Fourier transformation (IFT) method,[13] we found a number-weighted radius of $R_{n,IFT}$ = 3.0 ± 0.1 nm, a volume-weighted radius $R_{v,IFT}$ = 3.4 ± 0.1 nm, and a σ_{IFT} = 0.6 ± 0.1 nm (Figure SI2). The use of the recently published Monte Carlo-based data evaluation program McSAS[14] results in $R_{n,MC}$ = 3.1 ± 0.1 nm, $R_{v,MC}$ = 3.4 ± 0.1 nm, and σ_{MC} = 0.6 ± 0.1 nm (Figure SI3). Therefore, the three different data evaluation methods for SAXS data interpretation produce consistent results. We conclude that the core radii are independent of the stabilizer used. This is supported by electron microscopy pictures showing a mean particle radius of $R_{n,TEM}$ = 3.0 nm (see Figure SI4). In the following we refer only to R_n. Estimates of the shell thickness can now be drawn from the difference between the particle's hydrodynamic radius and its core radius $R_{shell} = R_H - R_n$, resulting in R_{shell} = 2.9 ± 0.2 nm ($\mathbf{p}_{Hu}$), 7.0 ± 0.2 nm ($\mathbf{p}_{PAA}$), 3.8 ± 0.2 nm ($\mathbf{p}_{GSH}$), and 8.9 ± 0.5 nm ($\mathbf{p}_{BSA}$).

Knowledge of the particle concentration is important for the application as reference material. The particle number concentration in the parent particle solution of $\mathbf{p}_{PAA}$ as determined by SASfit[12] is c_n = (2.2 ± 0.1) × 10^{15} or (4.4 ± 0.2) × 10^{-6} mol L^{-1}, which correspond to a volume concentration of c_v = 3.1 ± 0.1 g L^{-1}, in agreement with results from McSAS. We double checked this results first by evaluation of density measurements, which provide $c_{v,densiy}$ = 3.0 ± 0.1 g L^{-1}, and second by atomic absorption spectroscopy, which provides $c_{v,AAS}$ = 3.006 ± 0.010 g L^{-1}.

To summarize the SAXS analysis, we found that $\mathbf{p}_{Hu}$, $\mathbf{p}_{PAA}$, $\mathbf{p}_{GSH}$, and $\mathbf{p}_{BSA}$ display the same narrow core size distribution with a number-weighted radius of 3.0 nm. The ligand exchange of PAA with GSH and BSA was successful without formation of aggregates. Because of its instability, we omitted $\mathbf{p}_{Hu}$ for the following investigations and concentrate on $\mathbf{p}_{PAA}$ and its derivatives.

Optical Properties. *FTIR.* The colloidal stability of $\mathbf{p}_{GSH}$ and $\mathbf{p}_{BSA}$ at pH 7 and the DLS results are strong indicators that PAA was removed from the surface of the particles when functionalized with GSH and BSA. However, these findings provide no direct evidence. Within this respect it is helpful that the carbonyl vibration band is very sensitive to binding of carboxyl groups to silver surfaces.[15] Therefore, we utilized FTIR on the carbonyl vibration band to detect PAA. The FTIR spectra of $\mathbf{p}_{PAA}$, $\mathbf{p}_{GSH}$, and $\mathbf{p}_{BSA}$ are shown in Figure 5, in which the vertical line indicates the position of the strong absorbance band of $\mathbf{p}_{PAA}$ with a maximum at 1723 cm^{-1}. This band is absent in the spectra of $\mathbf{p}_{GSH}$ and $\mathbf{p}_{BSA}$. We assign this vibration band to the carboxylate groups of PAA bound to the surface of the silver cores. Such has been also observed by Kumar et al.,[16] who detected carboxylic groups of a poly(acrylic acid) on the surface of silver nanoparticles. A detailed discussion of the FITR spectra of PAA silver nanocomposites is given by Chalal et al.[17] Further, Cardenas et al.[18] investigated PAA on the surface of metal clusters and reported shifts of the carbonyl vibration band between 1717 and 1752 cm^{-1} depending on the cluster. Here we want to restrict our discussion to the point that the absence of the carbonyl band of PAA at around 1723 cm^{-1}

DOI: 10.1021/acs.langmuir.6b01477
Langmuir 2016, 32, 7383−7391

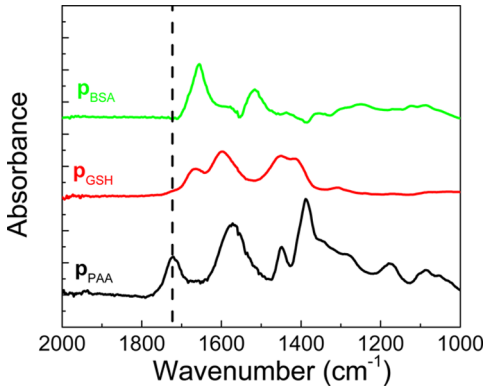

Figure 5. FTIR spectra of $\mathbf{p}_{PAA}$, $\mathbf{p}_{GSH}$, and $\mathbf{p}_{BSA}$. The dashed line indicates the position of the strong absorbance band of $\mathbf{p}_{PAA}$ with a maximum at 1723 cm^{-1}, which is absent in the spectra of $\mathbf{p}_{GSH}$ and $\mathbf{p}_{BSA}$.

in the spectra of $\mathbf{p}_{GSH}$ and $\mathbf{p}_{BSA}$ serves as a direct evidence for the replacement of PAA as stabilizer by GSH and BSA, respectively.

UV–Vis. The $\mathbf{p}_{PAA}$ particles display an intense UV–vis absorbance peak with a maximum at λ_{max} = 412 nm and a full width at half-maximum fwhm = 58 nm (Figure 6). This is the typical surface plasmon resonance band of very small silver nanoparticles, in agreement with the literature.[8] In the case of $\mathbf{p}_{GSH}$ the peak shifts to a shorter wavelength of λ_{max} = 404 nm and broadens slightly to fwhm = 72 nm. In contrast, the peak of $\mathbf{p}_{BSA}$ is shifted to a larger wavelength of λ_{max} = 418 nm while the peak width of fwhm = 61 nm is nearly the same as for $\mathbf{p}_{PAA}$. The peak shifts indicate that PAA was successfully replaced by GSH and BSA, respectively, because it is well-known that silver nanoparticles with different stabilizers can have quite different absorbance spectra even for the same particle size distribution.[19]

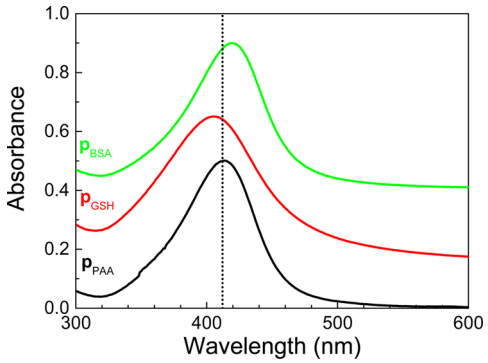

Figure 6. UV–vis spectrum of $\mathbf{p}_{PAA}$ (black line) in water with a peak maximum at a wavelength of 412 nm (position is indicated by dotted line) and a fwhm of 58 nm. The maxima of $\mathbf{p}_{GSH}$ (red line) and $\mathbf{p}_{BSA}$ (green line) are at 404 and 418 nm, respectively. The corresponding fwhm values are 72 and 61 nm. Curves are shifted vertically for better visibility.

Shifts of the surface plasmon band are attributed to changes in the refractive index of the particles' surroundings which happen when the shell composition changes.[19] Qualitatively, a hydrophobically bound stabilizer shifts the plasmon band to larger wavelength. This is in agreement with our findings for $\mathbf{p}_{BSA}$, since BSA is much more hydrophobic than PAA and therefore could explain the small red-shift of $\Delta\lambda_{max}$ = +6 nm. It has been reported that the binding of human serum albumin to Au/Ag alloy particles produced also a red-shift from 410 nm to about 416 nm when citrate is replaced by human serum albumin.[20] Alarcon et al. found also that BSA produces a small red-shift of the peak maximum of silver particles.[21] The small blue-shift of $\Delta\lambda_{max}$ = −8 nm when PAA is replaced by GSH can be explained similar.[20] The GSH contains a −SH group which has a strong affinity to silver surfaces, and this is very likely the reason for the small shift of λ_{max} and the slight broadening of the fwhm. The UV spectrum of $\mathbf{p}_{GSH}$ is visually the same as the spectrum of GSH stabilized silver nanoparticles reported by Li et al.[22] In all cases, the absence of a striking broadening of the UV bands of $\mathbf{p}_{GSA}$ and $\mathbf{p}_{BSA}$ in comparison to $\mathbf{p}_{PAA}$ confirms the absence of a significant amount of aggregates.

Catalytic Properties. We investigated the catalytic properties of $\mathbf{p}_{PAA}$, $\mathbf{p}_{GSH}$, and $\mathbf{p}_{BSA}$ by utilizing the reduction of 4-nitrophenol to 4-aminophenol with sodium borohydride. This reaction functions as a "gold standard" for investigating the catalytic properties of nanoparticles made of silver, gold, palladium, etc.[23] For ease of comparison, we used the same experimental conditions as applied by Fenger et al.,[24] who investigated the size dependency of the catalytic activity of CTAB-stabilized gold nanoparticles.[24] They found that not the expected smallest, but medium-sized nanoparticles with a radius of 6.5 nm were the most efficient. These particles display a higher catalytic activity than smaller (5 and 2.8 nm) and larger

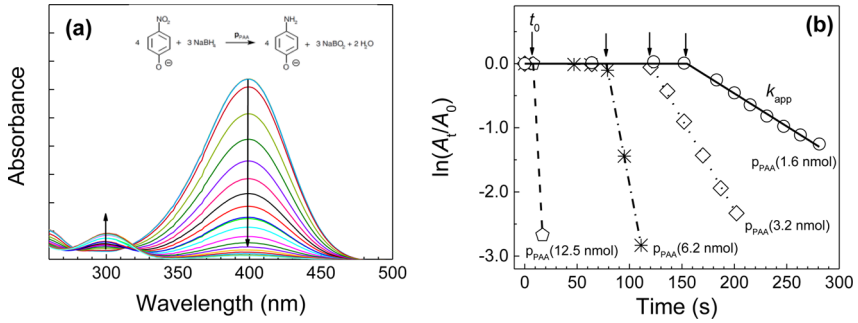

Figure 7. (a) UV–vis spectra of the catalytic process of 4-nitrophenolate to 4-aminophenolate in water after adding 1.6 nmol of silver ($\mathbf{p}_{PAA}$). The concentration of silver in the reaction solution was 3.9×10^{-7} mol L^{-1} (4.2×10^{-5} g L^{-1}). Concentration of 4-nitrophenolate was 6.6×10^{-5} mol L^{-1}, and that of sodium borohydride was 3.3×10^{-5} mol L^{-1}. The main peak at 400 nm indicating 4-nitrophenolate ions is decreasing with reaction time while the peak at 300 nm of 4-aminophenolate is increasing (indicated by arrows). (b) Comparison of the catalytic activity of $\mathbf{p}_{PAA}$ after adding an amount of 12.5, 6.2, 3.2, or 1.6 nmol of silver. The induction periods, t_0, are indicated by arrows; the apparent reaction constants, k_{app}, correspond to the linear slope in each curve. The lines are fit curves from applying eq 1.

DOI: 10.1021/acs.langmuir.6b01477
Langmuir 2016, 32, 7383–7391

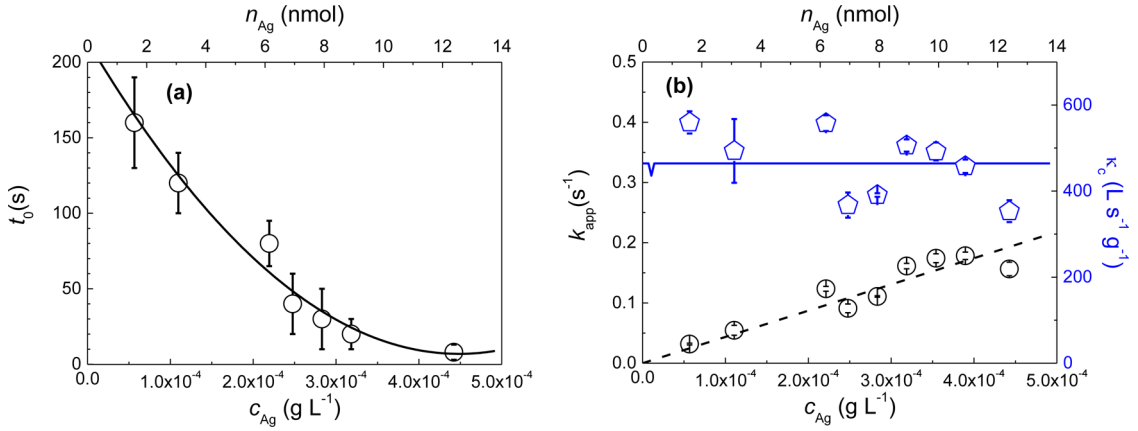

Figure 8. (a) Induction period t_0 as a function of the concentration of $\mathbf{p}_{PAA}$ (circles) and its approximation by a quadratic polynomial (solid line): $t_0 = 214 \pm 23$ s $- (9.2 \pm 1.6) \times 10^5$ L s $g^{-1} \times (c_{Ag}) + (1.1 \pm 0.2) \times 10^9$ L^2 s $g^{-2} \times (c_{Ag})^2$. (b) Apparent reaction constant k_{app} as a function of the added amount of $\mathbf{p}_{PAA}$ (circles) and its approximation by a linear relationship (black dashed line): $k_{app} = 436 \pm 23$ L s^{-1} $g^{-1} \times c_{Ag}$. The reaction parameter κ_c as a function of the concentration (blue octagons) can be approximated by a constant of $\kappa_c = 436 \pm 23$ L s^{-1} g^{-1} (blue solid line).

particles (14 and 28 nm). Therefore, the catalytic activity of metal nanoparticles does not necessarily increase with decreasing size, potentially due to the strong curvature of the surface of very small particles. That means that the very small size of our silver particles is not a guarantee for a high catalytic efficiency.

We started the investigation of our nanoparticles by adding 50 μL of $\mathbf{p}_{PAA}$ with a total amount of 12.5 nmol silver to 3 mL of a solution containing 4-nitrophenol and sodium borohydride. The silver concentration in the reaction mixture was therefore 3.2×10^{-4} g L^{-1} (3.0×10^{-6} mol L^{-1}). The sodium borohydride leads to a basic pH and a yellow solution of 4-nitrophenolate which is stable for hours if no $\mathbf{p}_{PAA}$ is added. We found that the yellow color of the solution decolorized within seconds after adding the nanoparticles (see video of this reaction in the Supporting Information). After a reaction time of 20−30 s, no 4-nitrophenol could be detected by UV−vis spectroscopy, which approximately corresponds to a rate constant of 0.3 ± 0.1 s^{-1}. From this number we estimate that the $\mathbf{p}_{PAA}$ particles are about 60-fold higher catalytically active than the 6.5 nm gold nanoparticles of Fenger et al.,[24] which have a rate constant of $(6.1 \pm 0.1) \times 10^{-3}$ s^{-1}.

With the surprisingly high catalytic activity of $\mathbf{p}_{PAA}$ we focused on the catalytic properties in order to be able to quantify the reaction kinetics with UV−vis properly. Therefore, we reduced the amount of added $\mathbf{p}_{PAA}$ nanoparticles stepwise in the line 12.5, 6.2, 3.2 to 1.6 nmol of silver to monitor the decolorization more precisely. The resulting UV−vis spectra of the catalytic process of 4-nitrophenolate to 4-aminophenolate after adding $\mathbf{p}_{PAA}$ particles (1.6 nmol of silver) are shown in Figure 7a. Therein, the main peak of 4-nitrophenolate ions at 400 nm is decreasing with reaction time, while the second peak at 300 nm of 4-aminophenolate is slowly increasing (indicated by arrows). Two isosbestic points are visible at 280 and 314 nm. The time dependence of the absorbance of 4-nitrophenolate ions at 400 nm is characterized by an induction period t_0, wherein the absorbance is constant, followed by a linear decrease. This is shown in Figure 7b for different amounts of added $\mathbf{p}_{PAA}$. The absorbance can therefore be quantified by t_0 and an apparent reaction constant, k_{app}, as

$$\ln\left(\frac{A}{A_0}\right)(t) = 0 \quad \text{for } t \le t_0,$$
$$\ln\left(\frac{A}{A_0}\right)(t) = \ln\left(\frac{A}{A_0}\right)(0) - k_{app}t \quad \text{for } t > t_0 \tag{1}$$

The induction periods are obtained as

$$t_0 = \frac{\ln\left(\frac{A}{A_0}\right)(0)}{k_{app}}$$

Note that A_0 is the absorbance of the 4-nitrophenolate before $\mathbf{p}_{PAA}$ has been added. The ratio A/A_0 is identical to the ratio of the concentration of 4-nitrophenolate at time, t, to its concentration before the reaction starts, i.e., $A/A_0 = c/c_0$. Equation 1 therefore quantifies the relative change of the concentration of 4-nitrophenolate.

Typical results of fitting eq 1 to the experimental $\ln(A/A_0)(t)$ curves are shown in Figure 7b. It can be seen that t_0 decreases and k_{app} increases in the line of 1.6, 3.1, 6.2, and 12.5 nmol of added $\mathbf{p}_{PAA}$. The induction period as a function of the concentration of $\mathbf{p}_{PAA}$ is nonlinear and was approximated by a quadratic polynomial:

$$t_0 = (214 \pm 23) \text{ s} - (9.2 \pm 1.6) \times 10^5 \text{ L s } g^{-1} \times c_{Ag} + (1.0 \pm 0.2) \times 10^9 \text{ L}^2 \text{ s } g^{-2} \times {c_{Ag}}^2$$

as can be seen in Figure 8a (circles and solid line, respectively). Ballauff et al.[25] reported an induction period in all cases they studied when using gold/palladium alloy nanoparticles as catalyst with t_0 in their studies[26] typically around 20 s. They hypothesized that t_0 is related to a surface restructuring of the nanoparticles and supported this explanation with a study on gold nanoparticles.[27] But this theory is still under debate. Also, silver nanoparticles display an induction period, but it is typically not further discussed in the literature. For example, a t_0 of about 10^3 s was reported by Walker and Zaleski,[28] who embedded silver nanoparticles in the corona of magnetic nanoparticles. The largest t_0 time of silver nanoparticles we are aware of in the literature is about 1900 s, reported for Ag@SiO_2@Ag_{seeds} particles by Lee and Jang.[29] Therein the catalytic degradation of rhodamine B was chosen as model reaction.

DOI: 10.1021/acs.langmuir.6b01477
Langmuir 2016, 32, 7383−7391

Therefore, the presence of an induction period seems to be a general phenomenon in nanoparticle catalysis but is hardly investigated. We speculate that a low reproducibility of t_0 and the absence of reasonable physical understanding may explain this gap. In our opinion, t_0 is an important parameter for rating and understanding of nanoparticle's catalytic potential and therefore should be considered more closely in future studies.

The catalytic activity is strongly connected to the k_{app} and its dependence on the amount of used particles. It has to be expected that k_{app} increases with increasing amount of added $\mathbf{p}_{PAA}$ to the reaction mixture. More particles correspond simply to a larger total surface area of the catalyst and the availability of more active sites. A priori, we expected a linear increase of k_{app} with the amount of $\mathbf{p}_{PAA}$. The linear approximation of $k_{app} = 464 \pm 26\ L\ s^{-1}\ g^{-1} \times c_{Ag}$ is sufficiently fulfilled as can be seen in Figure 8b (dashed line). Lara et al.[30] recently reported also on a linear increase of k_{app} with increasing catalyst concentration but for a Fe_3O_4@dextran/Pd nanoparticle system. Many reported studies, however, use only a single concentration, making it impossible to draw further conclusions with respect to linearity.

Despite the widespread use of the 4-nitrophenol reaction, a direct comparison of our data with data from the literature is complicated by the variety of catalytic parameters that have been reported. Most of these studies simply report on k_{app} as summarized in a recent review by Zhao et al.[23] But k_{app} is dependent on the amount of silver nanoparticles used in the reaction. Therefore, the "activity parameter" κ is in use. The κ is often normalized with respect to the total mass of the catalyst added, κ_m, which ignores the reaction volume and consequently the catalyst concentration.[31] Thus, a second version of the "activity parameter", κ_c, is in use, which takes the mass of the catalyst and the volume of the reaction solution into account. To our opinion, κ_c, seems to be the most appropriate parameter for comparison of data from different studies.[30] For clarification, the κ_c is the ratio of k_{app} to the concentration of the metal catalyst in mass per volume, i.e., $[\kappa_c] = L\ g^{-1}\ s^{-1}$. In order to be sure not to overestimate the catalytic activity of $\mathbf{p}_{PAA}$, we use the mean value of $\kappa_c = 436 \pm 24\ L\ s^{-1}\ g^{-1}$ ($\mathbf{p}_{PAA}$) in the following, derived as shown in Figure 8b. We figured out that the activity parameter for $\mathbf{p}_{GSH}$ is only $77.6 \pm 0.9\ L\ s^{-1}\ g^{-1}$, which was measured for adding 1.6 nmol of silver. For $\mathbf{p}_{BSA}$ we even had to increase the amount of silver to 12.5 nmol to detect a significant catalytic activity of $3.47 \pm 0.50\ L\ s^{-1}\ g^{-1}$. A direct comparison of the experimental curves and the resulting activity parameters of $\mathbf{p}_{PAA}$, $\mathbf{p}_{GSH}$, and $\mathbf{p}_{BSA}$ are shown in Figures 9a and 9b.

We selected a few important studies from the literature for comparison with our findings. These are summarized together with our data in Table 1. First of all, Baruah et al. reported on silver nanoparticles with a radius of 9 nm stabilized by cationic polynorbornenes.[31] Therein they found $\kappa_m = 1375\ s^{-1}\ g^{-1}$, which they classified as significantly higher than other systems reported in the literature before 2013. This value corresponds to a normalized activity parameter of $\kappa_c = 1.375\ L\ s^{-1}\ g^{-1}$. As far as we know, this is still the highest published value for freely suspended silver particles. Quite recently, normalized activity parameters have been summarized by Zhang et al.[32] They reported a value of $\kappa_c = 4.38 \pm 0.37\ L\ s^{-1}\ g^{-1}$ for their silver nanoparticles which are stabilized in suspension on a support of sulfhydryl-functionalized poly(glycidyl methacrylate) microspheres. They classified them as the silver nanoparticles with the highest known κ_c for composite particles. Zheng et al.[33] reported on silver nanoparticles wrapped by an exopolysaccaride with radii of 2.5 nm and $\kappa_m = 15.75\ s^{-1}\ g^{-1}$, which corresponds to $\kappa_c = 0.047\ L\ s^{-1}\ g^{-1}$. This is an unexpectedly low value considering the small particles' size. A possible explanation could be the structure of this system. The structure model consists of an aggregate of exopolysaccaride chains with embedded silver nanoparticles forming a nanocomposite with a hydrodynamic radius of about 150 nm. Therein the reaction components must diffuse a relatively long path through exopolysaccaride aggregates before they reach the silver particles' surface. We speculate that this diffusion is the crucial step that lowers the catalytic activity. Patra et al. provided a comparison of selected silver nanoparticles with respect to their catalytic activity, and they studied silver nanoparticles embedded in porous poly(styrene) beads.[34] The radii of the pores and the silver particles are estimated below ca. 5 nm. The reported activity parameter is $\kappa_m = 974.07\ s^{-1}\ g^{-1}$, which corresponds to $\kappa_c = 1.95\ L\ s^{-1}\ g^{-1}$. This κ_c is surprisingly high and indicates that the surface of the silver nanoparticles is catalytically well accessible for the reactants. But this fast reaction starts not before 1000 s. Prior to that, an induction period of 400−500 s was observed followed by a period of slow reaction kinetics for several hundreds of seconds. It seems that the complex morphology of their system provides complex nano confinement effects which affect the reaction kinetics.

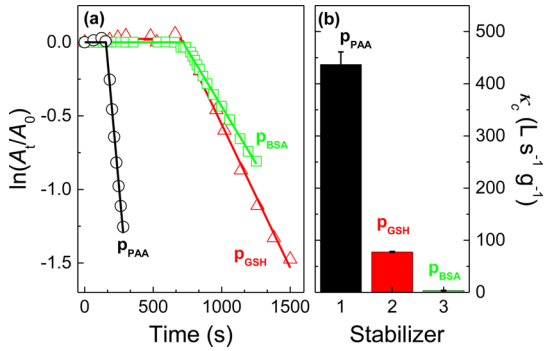

Figure 9. Comparison of the catalytic activity of $\mathbf{p}_{PAA}$, $\mathbf{p}_{GSH}$, and $\mathbf{p}_{BSA}$. (a) Time dependence of the absorbance of 4-nitrophenolate ions at 400 nm. The straight lines display the linear sections, from which the reaction constants k_{app} were determined. The added amounts of $\mathbf{p}_{PAA}$ and $\mathbf{p}_{GSH}$ were 1.6 nmol, while for $\mathbf{p}_{BSA}$ 12.5 nmol was added. (b) Activity parameters of the particles are $\kappa_c = 436 \pm 23\ L\ s^{-1}\ g^{-1}$ ($\mathbf{p}_{PAA}$), $77.6 \pm 0.9\ L\ s^{-1}\ g^{-1}$ ($\mathbf{p}_{GSH}$), and $3.47 \pm 0.50\ L\ s^{-1}\ g^{-1}$ ($\mathbf{p}_{BSA}$).

To the best of our knowledge, the κ_c for $\mathbf{p}_{PAA}$ is the highest value reported for silver nanoparticles. A substantially higher value of $\kappa_c = 3650\ L\ s^{-1}\ g^{-1}$ was reported for palladium nanoparticles with a radius of 3.9 nm by Lara et al.[30] The palladium nanoparticles were located on a dextran coating of magnetite particles.[30] This structure seems to make the metal surface very well accessible for the reactants.

We want to understand why the $\mathbf{p}_{PAA}$ display such a high catalytic activity. Surface area and accessibility have to be taken into account. The surface area of a silver nanoparticle with a radius of 3 nm is $10^3\ m^2\ cm^{-3}$, and the specific surface is $95\ m^2\ g^{-1}$ when assuming that the particles have the same density as silver in bulk form. The catalytic activity of the silver surface can now be normalized by the specific surface resulting in $\kappa_c/S_a = 4.58 \pm 0.25\ L\ m^{-2}\ s^{-1}$ ($\mathbf{p}_{PAA}$), $0.81 \pm 0.01\ L\ m^{-2}\ s^{-1}$ ($\mathbf{p}_{GSH}$), and $0.036 \pm 0.005\ L\ m^{-2}\ s^{-1}$ ($\mathbf{p}_{BSA}$). The S_a and κ_c/S_a values are summarized for all systems in Table 1. Compared with the κ_c/S_a values of the other catalytic systems, it becomes clear that even when normalized to the specific surface area the $\mathbf{p}_{PAA}$

DOI: 10.1021/acs.langmuir.6b01477
Langmuir 2016, 32, 7383−7391

Table 1. Comparison of Parameters of the Catalytic Reduction of 4-Nitrophenolate to 4-Aminophenolate from This Study and from the Literature[a]

nanoparticles	T (°C)	R_c (nm)	[Ag] (10^{-3} g L^{-1})	k_{app} (10^{-3} s^{-1})	κ_c (L s^{-1} g^{1-})	S_a (m^2 g^{-1})	κ_c/S_a (L $m^{-2}s^{-1}$)	ref
$\mathbf{p}_{PAA}$	22	3.0	0.035	15.46 ± 0.84	436 ± 24	95	4.58 ± 0.25	this work
$\mathbf{p}_{GSH}$	22	3.0	0.219	17.04 ± 0.19	77.7 ± 0.9	95	0.81 ± 0.01	this work
$\mathbf{p}_{BSA}$	22	3.0	0.442	1.53 ± 0.22	3.5 ± 0.5	95	0.036 ± 0.005	this work
Ag[b]	25	9	4.0	5.5	1.375	31	0.01	31
Ag[c]	RT	8.5	0.9	3.94 ± 0.33	4.38 ± 0.37	17	0.07	32
Ag[d]	25	2.5	0.0267	1.26	0.047	114	0.0001	33
Ag[e]	25	<5	0.0139	974.07	1.948	57	0.01	34
Pd[f]	15	3.9	0.0269	0.092	3650	6.3	151	30
Au[g]	25	6.5	0.807	0.0061	7.55	4	0.5	24

[a]Listed are temperature, T, particle radius, R_c, silver concentration, [Ag], apparent rate constant of the reaction, k_{app}, activity parameter, κ_c, specific surface area of the particles, S_a, and the activity parameter normalized by the specific surface area, κ_c/S_a. [b]Silver nanoparticles AgNP-PG-5K stabilized with a cationic polynorbornene, M_W = 5000 g mol^{-1}. [c]Silver nanoparticles AgNP@PGMA-SH stabilized with sulfhydryl functionalized poly(glycidyl methacrylate) microspheres. [d]Silver nanoparticles dispersed by a exopolysaccaride. [e]Silver nanoparticles embedded in porous poly(styrene) beads. [f]Palladium nanoparticles on the surface of Fe_3O_4@dextran particles. [g]Gold nanoparticles stabilized with cetyltrimethylammonium bromide.

particles are around 2 orders of magnitude more active than the other silver particle based systems. Only the palladium system has a much higher value of κ_c/S_a = 151 L m^{-2} s^{-1}, and for the gold nanoparticles the value is 0.5 L m^{-2} s^{-1}. It seems therefore reasonable to conclude that the silver surface of $\mathbf{p}_{PAA}$ particles is well accessible for the reactants through their water-swollen PAA shell, probably similar to the dextran shell of the palladium particles in the study of Lara et al.[30]

For a detailed kinetic study we refer to Ballauff et al.[35] They discussed bimetallic nanoparticles' activity parameters in detail,[36] and they found a κ_c/S_a = 1.10 L m^{-2} s^{-1} for palladium particles embedded in a cationic spherical polyelectrolyte brush.[37] We assume that the Langmuir−Hinshelwood model[35] may be suitable for our particles but this is beyond the scope of our current study.

Some researchers prefer to use the turnover frequency, k_{TOF}, instead of the activity parameter to quantify the catalytic activity of nanoparticles. The turnover frequency is the number of reactant molecules (4-nitrophenol) that 1 g of catalyst (Ag) can convert into product (4-aminophenol) per time.[38] Therefore, the turnover frequency for a first-order reaction can be calculated from the activity parameter by $k_{TOF} = \kappa_c c_{e,0} e^{-tc_c\kappa_c})$. The c_c is the concentration of the catalyst in g/L, and $c_{e,0}$ is the concentration of the educt 4-nitrophenol at t = 0 in molecules/L (without induction period). In the limit of short times we get $k_{TOF} = \kappa_c c_{e,0}$. The resulting k_{TOF} values are 28.78 ± 1.58 mmol g^{-1} s^{-1} for $\mathbf{p}_{PAA}$, 5.12 ± 0.06 mmol g^{-1} s^{-1} for $\mathbf{p}_{GSH}$, and 0.23 ± 0.03 mmol g^{-1} s^{-1} for $\mathbf{p}_{BSA}$. More clearly, these values correspond to reaction frequencies of 3.10 ± 0.17 4-nitrophenol molecules per silver atom and second for $\mathbf{p}_{PAA}$, 0.552 ± 0.006 for $\mathbf{p}_{GSH}$, and 0.025 ± 0.004 for $\mathbf{p}_{BSA}$.

CONCLUSIONS

We have shown that ultrasmall silver nanoparticles can be produced in large quantities which make their further use as reference material suitable. The particles are stable at ambient storage conditions for more than 6 months. The original PAA stabilizer can be easily replaced by other stabilizers to tune the surface on demand, as has been demonstrated by using BSA and glutathione. Of interest is that the parent PAA stabilized particles display the highest catalytic activity of silver nanoparticles reported to date for the reduction of 4-nitrophenolate to 4-amionophenolate. The particles are available from the authors on request.

MATERIALS AND METHODS

Materials. Water used for all preparations was Milli-Q grade (18.2 MΩ at 25 °C). All chemicals were used as received and without further purification. Silver nitrate was purchased from AppliChem, ethylene glycol from Acros, glutathione from Merck, 4-nitrophenol from Fluka, and poly(acrylic) acid (catalog number 323667-250g), BSA, and sodium borohydride from Sigma-Aldrich.

Synthesis. The polyol process for silver nanoparticles was adapted from Hu et al.[8] Briefly, solution 1 was prepared by solving 1.944 g (11.444 mmol) of silver nitrate under stirring in 58.5 mL of ethylene glycol at room temperature. Solution 2 was prepared by adding 15.7 g (217.9 mmol with respect to the monomer units) of poly(acrylic acid) to 291.5 mL of ethylene glycol and heating the mixture under stirring to 200 °C. A short chain poly(acrylic acid) with a molar mass of M_w = 1800 g mol^{-1} was chosen, which contains 25 monomer units per polymer chain. The ratio of silver ions to acrylic acid monomer units was 1 to 19. The solution 1 was added within 3 s to the boiling solution 2 under rigorous stirring. The mixture was boiled for 15 min and was then cooled down to room temperature. The processing of the particles started by adding 800 mL of water with a pH value of 5 and storing of the mixture for 24 h. Then the reddish-brown supernatant was decanted. This procedure was repeated three times. Then, the residue was suspended with 150 mL of water, and a 1% (w/v) sodium hydroxide solution was added in drops until the pH of the dispersion is adjusted to 10. The color turned from starting with reddish-brown via olive-green to brownish-black. The amount of PAA in the final dispersion was 13% (w/w) as determined with TGA measurements. Note that the samples were dried at 80 °C before TGA measurement to remove the water.

Functionalization of Particles with GSH and BSA. For the ligand exchange with BSA 1 mL of the parent particle dispersion was placed in a glass vial, and 1.5 mL of 10^{-4} M BSA solution was added. The mixture was stirred for 5 days.

For the transfunctionalization with GSH a solution of 6 × 10^{-3} M glutathione in 1% (w/v) sodium hydroxide solution was prepared. 1.075 mL of the GSH solution was added to 2.5 mL of the parent particle dispersion ($\mathbf{p}_{PAA}$) and stirred for 5 days.

DLS Measurements. The DLS measurements were performed using a multiangle ALV Instrument (ALV 7004, ALV Langen) equipped with a He−Ne laser (λ = 632.8 nm). The scattering data were recorded at 23 ± 1 °C at scattering angles of 2θ = 26°−146° (8° steps). We measured six runs with 60 s for each angle. For measurement the samples were diluted 1:100 with water ($\mathbf{p}_{BSA}$, $\mathbf{p}_{GSH}$) and sodium hydroxide solution with a pH of 10 ($\mathbf{p}_{PAA}$). We applied the standardized method of cumulants[39,40] for determination of the hydrodynamic radii at different angles, which produces realistic values for R_H if the polydispersity index (PDI) is lower than 0.1. The PDI is defined as the ratio of the variance of the relaxation rates (second cumulant = μ) to the square of the mean relaxation rate (first

DOI: 10.1021/acs.langmuir.6b01477
Langmuir 2016, 32, 7383−7391

cumulant $\bar{\Gamma}$): PDI = $\mu/\bar{\Gamma}^2$. Further, the linear extrapolation of $1/R_h$ as a function of q^2 toward $1/R_h(q = 0)$ is a proven method for determination of R_h of polydisperse samples.[11]

SAXS Measurements. SAXS measurements were performed in a flow-through capillary with a Kratky-type instrument (SAXSess from Anton Paar, Austria) at 21 ± 1 °C. The SAXSess has a low sample-to-detector distance of 0.309 m, which is appropriate for investigation of dispersions with low scattering intensities. The measured intensity was converted to absolute scale according to Orthaber et al.[41] The scattering vector is defined in terms of the scattering angle q and the wavelength λ of the radiation (λ = 0.154 nm): thus, $q = 4\pi n/\lambda \sin\theta$. Deconvolution (slit length desmearing) of the SAXS curves was performed with the SAXS-Quant software. Samples analyzed with SAXS were used as prepared. Curve fitting was conducted with software SASfit,[12] curve simulation by Monte Carlo methods with the software McSAS,[42] and Glatter's indirect Fourier transformation method which is based on regularization.[13]

TEM Imaging. The TEM images were obtained from a FEI Tecnai TF 20 X-TWIN transmission electron microscope operating at 200 kV.

UV–Vis. UV–vis absorbance spectra were measured using a Cary 300 Scan double-beam spectrometer from Varian. The dispersions were diluted 1:100 with water ($\mathbf{p}_{BSA}$, $\mathbf{p}_{GSH}$) and sodium hydroxide solution with a pH of 10 ($\mathbf{p}_{PAA}$).For the measurements 2.5 mL disposable cuvettes (PMMA) with a path length of 1 cm from Brand were used. The background correction was done with deionized water as reference. The background correction was done with deionized water as reference.

Catalytic Reaction. A standard catalytic test reaction as used by Fenger et al.[24] was carried out in 4.5 mL quartz cuvettes with a path length of 1 cm. A volume of 2 mL aqueous solution of 10^{-4} M 4-nitrophenol was mixed with 1 mL of 10^{-1} M sodium borohydride solution. The reaction was started with the addition of 50 μL of nanoparticle dispersion. For clarification, the addition 1 nmol of silver (atoms) corresponds to a silver concentration of 3.5377×10^{-5} g L^{-1} in the volume of the reaction mixture. Immediately after particle addition, time-dependent adsorption spectra were collected at a temperature of 22 °C. The background correction was done with deionized water as reference.

■ ASSOCIATED CONTENT

Supporting Information

The Supporting Information is available free of charge on the ACS Publications website at DOI: 10.1021/acs.langmuir.6b01477.

Figures S1–S4 (PDF)

Video showing yellow color of the 4-nitrophenol–sodium borohydride solution decolorized within seconds after adding the nanoparticles (AVI)

■ AUTHOR INFORMATION

Corresponding Author

*E-mail andreas.thuenemann@bam.de; Tel +493081041610 (A.F.T.).

Notes

The authors declare no competing financial interest.

■ ACKNOWLEDGMENTS

We thank M. Ebisch for repeating the particle synthesis many times. We also thank Dr. M. Gajewska from the Centre for Materials and Nanotechnology (ACMiN) at AGH University of Science and Technology in Krakow for the TEM images. We gratefully thank D. Lichtenstein from the Federal Institute for Risk Assessment (BfR) for the AAS measurements. M.-L. Heinrich helped in performing the catalysis experiments. We also thank D. Neubert for performing the TGA measurements, P. Fengler for her assistance with DLS measurements, and B. R. Pauw for discussing the manuscript.

■ REFERENCES

(1) Lu, Y. Z.; Wang, Y. C.; Chen, W. Silver nanorods for oxygen reduction: Strong effects of protecting ligand on the electrocatalytic activity. *J. Power Sources* **2011**, *196*, 3033–3038.

(2) Chaloupka, K.; Malam, Y.; Seifalian, A. M. Nanosilver as a new generation of nanoproduct in biomedical applications. *Trends Biotechnol.* **2010**, *28*, 580–588.

(3) Chernousova, S.; Epple, M. Silver as antibacterial agent: ion, nanoparticle, and metal. *Angew. Chem., Int. Ed.* **2013**, *52*, 1636–53.

(4) Xiu, Z. M.; Zhang, Q. B.; Puppala, H. L.; Colvin, V. L.; Alvarez, P. J. J. Negligible Particle-Specific Antibacterial Activity of Silver Nanoparticles. *Nano Lett.* **2012**, *12*, 4271–4275.

(5) Haase, A.; Rott, S.; Mantion, A.; Graf, P.; Plendl, J.; Thunemann, A. F.; Meier, W. P.; Taubert, A.; Luch, A.; Reiser, G. Effects of Silver Nanoparticles on Primary Mixed Neural Cell Cultures: Uptake, Oxidative Stress and Acute Calcium Responses. *Toxicol. Sci.* **2012**, *126*, 457–468.

(6) Stefaniak, A. B.; Hackley, V. A.; Roebben, G.; Ehara, K.; Hankin, S.; Postek, M. T.; Lynch, I.; Fu, W. E.; Linsinger, T. P. J.; Thunemann, A. F. Nanoscale reference materials for environmental, health and safety measurements: needs, gaps and opportunities. *Nanotoxicology* **2013**, *7*, 1325–1337.

(7) Desireddy, A.; Conn, B. E.; Guo, J. S.; Yoon, B.; Barnett, R. N.; Monahan, B. M.; Kirschbaum, K.; Griffith, W. P.; Whetten, R. L.; Landman, U.; Bigioni, T. P. Ultrastable silver nanoparticles. *Nature* **2013**, *501*, 399–402.

(8) Hu, Y. X.; Ge, J. P.; Lim, D.; Zhang, T. R.; Yin, Y. D. Size-controlled synthesis of highly water-soluble silver nanocrystals. *J. Solid State Chem.* **2008**, *181*, 1524–1529.

(9) Ehlert, S.; Taheri, S. M.; Pirner, D.; Drechsler, M.; Schmidt, H. W.; Forster, S. Polymer Ligand Exchange to Control Stabilization and Compatibilization of Nanocrystals. *ACS Nano* **2014**, *8*, 6114–6122.

(10) Lu, X. H.; Tan, C. Y.; Xu, J. W.; He, C. B. Thermal degradation of electrical conductivity of polyacrylic acid doped polyaniline: effect of molecular weight of the dopants. *Synth. Met.* **2003**, *138*, 429–440.

(11) Bantz, C.; Koshkina, O.; Lang, T.; Galla, H. J.; Kirkpatrick, C. J.; Stauber, R. H.; Maskos, M. The surface properties of nanoparticles determine the agglomeration state and the size of the particles under physiological conditions. *Beilstein J. Nanotechnol.* **2014**, *5*, 1774–1786.

(12) Bressler, I.; Kohlbrecher, J.; Thunemann, A. F. SASfit: a tool for small-angle scattering data analysis using a library of analytical expressions. *J. Appl. Crystallogr.* **2015**, *48*, 1587–1598.

(13) Glatter, O. Determination of Particle-Size Distribution-Functions from Small-Angle Scattering Data by Means of the Indirect Transformation Method. *J. Appl. Crystallogr.* **1980**, *13*, 7–11.

(14) Bressler, I.; Pauw, B. R.; Thunemann, A. F. McSAS: software for the retrieval of model parameter distributions from scattering patterns. *J. Appl. Crystallogr.* **2015**, *48*, 962–969.

(15) Yin, B. S.; Ma, H. Y.; Wang, S. Y.; Chen, S. H. Electrochemical synthesis of silver nanoparticles under protection of poly(N-vinylpyrrolidone). *J. Phys. Chem. B* **2003**, *107*, 8898–8904.

(16) Kumar, V.; Jolivalt, C.; Pulpytel, J.; Jafari, R.; Arefi-Khonsari, F. Development of silver nanoparticle loaded antibacterial polymer mesh using plasma polymerization process. *J. Biomed. Mater. Res., Part A* **2013**, *101*, 1121–1132.

(17) Chalal, S.; Haddadine, N.; Bouslah, N.; Benaboura, A. Preparation of Poly(acrylic acid)/silver nanocomposite by simultaneous polymerization-reduction approach for antimicrobial application. *J. Polym. Res.* **2012**, *19*, 24.

(18) Cardenas, G.; Munoz, C.; Carbacho, H. Thermal properties and TGA-FTIR studies of polyacrylic and polymethacrylic acid doped with metal clusters. *Eur. Polym. J.* **2000**, *36*, 1091–1099.

(19) Mulvaney, P. Surface plasmon spectroscopy of nanosized metal particles. *Langmuir* **1996**, *12*, 788–800.

(20) Sharma, A. S.; Ilanchelian, M. Comprehensive Multispectroscopic Analysis on the Interaction and Corona Formation of Human

DOI: 10.1021/acs.langmuir.6b01477
Langmuir 2016, 32, 7383–7391

Serum Albumin with Gold/Silver Alloy Nanoparticles. *J. Phys. Chem. B* **2015**, *119*, 9461−9476.
(21) Alarcon, E. I.; Bueno-Alejo, C. J.; Noel, C. W.; Stamplecoskie, K. G.; Pacioni, N. L.; Poblete, H.; Scaiano, J. C. Human serum albumin as protecting agent of silver nanoparticles: role of the protein conformation and amine groups in the nanoparticle stabilization. *J. Nanopart. Res.* **2013**, *15*, 1374.
(22) Li, H. B.; Cui, Z. M.; Han, C. P. Glutathione-stabilized silver nanoparticles as colorimetric sensor for Ni(2+) ion. *Sens. Actuators, B* **2009**, *143*, 87−92.
(23) Zhao, P. X.; Feng, X. W.; Huang, D. S.; Yang, G. Y.; Astruc, D. Basic concepts and recent advances in nitrophenol reduction by gold- and other transition metal nanoparticles. *Coord. Chem. Rev.* **2015**, *287*, 114−136.
(24) Fenger, R.; Fertitta, E.; Kirmse, H.; Thunemann, A. F.; Rademann, K. Size dependent catalysis with CTAB-stabilized gold nanoparticles. *Phys. Chem. Chem. Phys.* **2012**, *14*, 9343−9.
(25) Gu, S.; Lu, Y.; Kaiser, J.; Albrecht, M.; Ballauff, M. Kinetic analysis of the reduction of 4-nitrophenol catalyzed by Au/Pd nanoalloys immobilized in spherical polyelectrolyte brushes. *Phys. Chem. Chem. Phys.* **2015**, *17*, 28137−28143.
(26) Wunder, S.; Polzer, F.; Lu, Y.; Mei, Y.; Ballauff, M. Kinetic Analysis of Catalytic Reduction of 4-Nitrophenol by Metallic Nanoparticles Immobilized in Spherical Polyelectrolyte Brushes. *J. Phys. Chem. C* **2010**, *114*, 8814−8820.
(27) Wunder, S.; Lu, Y.; Albrecht, M.; Ballauff, M. Catalytic Activity of Faceted Gold Nanoparticles Studied by a Model Reaction: Evidence for Substrate-Induced Surface Restructuring. *ACS Catal.* **2011**, *1*, 908−916.
(28) Walker, J. M.; Zaleski, J. M. A simple route to diverse noble metal-decorated iron oxide nanoparticles for catalysis. *Nanoscale* **2016**, *8*, 1535−1544.
(29) Lee, J.; Jang, D. W. Highly Efficient Catalytic Performances of Eco-Friendly Grown Silver Nanoshells. *J. Phys. Chem. C* **2016**, *120*, 4130−4138.
(30) Lara, L. R. S.; Zottis, A. D.; Elias, W. C.; Faggion, D.; de Campos, C. E. M.; Acuna, J. J. S.; Domingos, J. B. The catalytic evaluation of in situ grown Pd nanoparticles on the surface of Fe_3O_4@ dextran particles in the p-nitrophenol reduction reaction. *RSC Adv.* **2015**, *5*, 8289−8296.
(31) Baruah, B.; Gabriel, G. J.; Akbashev, M. J.; Booher, M. E. Facile Synthesis of Silver Nanoparticles Stabilized by Cationic Polynorbornenes and Their Catalytic Activity in 4-Nitrophenol Reduction. *Langmuir* **2013**, *29*, 4225−4234.
(32) Zhang, W. C.; Sun, Y.; Zhang, L. In Situ Synthesis of Monodisperse Silver Nanoparticles on Sulfhydryl-Functionalized Poly(glycidyl methacrylate) Microspheres for Catalytic Reduction of 4-Nitrophenol. *Ind. Eng. Chem. Res.* **2015**, *54*, 6480−6488.
(33) Zheng, Z. M.; Huang, Q. L.; Guan, H.; Liu, S. Y. In situ synthesis of silver nanoparticles dispersed or wrapped by a Cordyceps sinensis exopolysaccharide in water and their catalytic activity. *RSC Adv.* **2015**, *5*, 69790−69799.
(34) Patra, S.; Pandey, A. K.; Sarkar, S. K.; Goswami, A. Wonderful nanoconfinement effect on redox reaction equilibrium. *RSC Adv.* **2014**, *4*, 33366−33369.
(35) Gu, S.; Wunder, S.; Lu, Y.; Ballauff, M.; Fenger, R.; Rademann, K.; Jaquet, B.; Zaccone, A. Kinetic Analysis of the Catalytic Reduction of 4-Nitrophenol by Metallic Nanoparticles. *J. Phys. Chem. C* **2014**, *118*, 18618−18625.
(36) An, Q.; Yu, M.; Zhang, Y. T.; Ma, W. F.; Guo, J.; Wang, C. C. Fe_3O_4@Carbon Microsphere Supported Ag-Au Bimetallic Nanocrystals with the Enhanced Catalytic Activity and Selectivity for the Reduction of Nitroaromatic Compounds. *J. Phys. Chem. C* **2012**, *116*, 22432−22440.
(37) Mei, Y.; Lu, Y.; Polzer, F.; Ballauff, M.; Drechsler, M. Catalytic activity of palladium nanoparticles encapsulated in spherical polyelectrolyte brushes and core-shell microgels. *Chem. Mater.* **2007**, *19*, 1062−1069.
(38) Saha, S.; Pal, A.; Kundu, S.; Basu, S.; Pal, T. Photochemical Green Synthesis of Calcium-Alginate-Stabilized Ag and Au Nanoparticles and Their Catalytic Application to 4-Nitrophenol Reduction. *Langmuir* **2010**, *26*, 2885−2893.
(39) Koppel, D. E. Analysis of Macromolecular Polydispersity in Intensity Correlation Spectroscopy - Method of Cumulants. *J. Chem. Phys.* **1972**, *57*, 4814−4820.
(40) ISO.Particle size analysis - Photon correlation spectroscopy - ISO 13321:1996(E) International Organization for Standardization 1996, ISO 13321:1996(E).
(41) Orthaber, D.; Bergmann, A.; Glatter, O. SAXS experiments on absolute scale with Kratky systems using water as a secondary standard. *J. Appl. Crystallogr.* **2000**, *33*, 218−225.
(42) Pauw, B. R. Everything SAXS: small-angle scattering pattern collection and correction. *J. Phys.: Condens. Matter* **2013**, *25*, 383201.

DOI: 10.1021/acs.langmuir.6b01477
Langmuir 2016, 32, 7383−7391